Origin of multistate resistive switching in Ti/manganite/SiO_X/Si heterostructures

W. Román Acevedo, C. Acha, M. J. Sánchez, P. Levy, and D. Rubi

Citation: Appl. Phys. Lett. **110**, 053501 (2017); doi: 10.1063/1.4975157
View online: http://dx.doi.org/10.1063/1.4975157
View Table of Contents: http://aip.scitation.org/toc/apl/110/5
Published by the American Institute of Physics

Origin of multistate resistive switching in Ti/manganite/SiO_x/Si heterostructures

W. Román Acevedo,[1,2] C. Acha,[2,3] M. J. Sánchez,[2,4] P. Levy,[1,2] and D. Rubi[1,2,5,a)]
[1]*Gerencia de Investigación y Aplicaciones, CNEA, Av. Gral Paz 1499, San Martín, 1650 Buenos Aires, Argentina*
[2]*Consejo Nacional de Investigaciones Científicas y Técnicas (CONICET), Godoy Cruz 2290, 1425 Buenos Aires, Argentina*
[3]*Depto. de Física, FCEyN, Universidad de Buenos Aires & IFIBA-CONICET, Pab I, Ciudad Universitaria, 1428 Buenos Aires, Argentina*
[4]*Centro Atómico Bariloche and Instituto Balseiro, 8400 San Carlos de Bariloche, Río Negro, Argentina*
[5]*Escuela de Ciencia y Tecnología, UNSAM, Campus Miguelete, San Martín, 1650 Buenos Aires, Argentina*

(Received 19 October 2016; accepted 18 January 2017; published online 30 January 2017)

We report on the growth and characterization of Ti/$La_{1/3}Ca_{3/2}MnO_3$/SiO_2/n-Si memristive devices. We demonstrate that using current as electrical stimulus unveils an intermediate resistance state, in addition to the usual high and low resistance states that are observed in the standard voltage controlled experiments. Based on thorough electrical characterization (impedance spectroscopy, current-voltage curves analysis), we disclose the contribution of three different microscopic regions of the device to the transport properties: an ohmic incomplete metallic filament, a thin manganite layer below the filament tip exhibiting Poole-Frenkel like conduction, and the SiO_x layer with an electrical response well characterized by a Child-Langmuir law. Our results suggest that the existence of the SiO_x layer plays a key role in the stabilization of the intermediate resistance level, indicating that the combination of two or more active resistive switching oxides adds functionalities in relation to the single-oxide devices. We understand that these multilevel devices are interesting and promising, as their fabrication procedure is rather simple and they are fully compatible with the standard Si-based electronics. *Published by AIP Publishing*. [http://dx.doi.org/10.1063/1.4975157]

The continuous increase in memory densities over the last decades has been, to a large extent, responsible for the impressive evolution of new micro- and nanoelectronic devices. Further progress, especially in mobile appliances, crucially depends on new developments in solid-state memories. New memory devices should combine non-volatility, speed, durability and extended scaling. Different technologies have been proposed to accomplish these requirements, such as phase-change memories, magnetic or ferroelectric random access memories and resistive random access memories (RRAM). The latter are based on metal/insulator/metal or metal/insulator/semiconductor structures, usually called "memristors," which display a significant, non-volatile change in their resistance upon application of electrical stress. This effect was named resistive switching (RS) since early 00's (see reviews Refs. 1 and 2 and references therein). RS has been found to ubiquitously exist in a huge variety of simple and complex transition metal oxides, and it shows promising properties in terms of scalability, low power consumption and fast write/read access times. In addition, memristors were shown to behave similarly to human brain bit-cells (synapses),[3,4] suggesting the possibility of developing disruptive devices with neuromorphic behaviour. Thus, additional functionalities foster the search of selected oxides that could potentiate memory device capabilities.

Massive Si planar technology prompts the use of heavily doped Si substrates as the bottom electrode (instead of a metal) in memristive stacks. Naturally, SiO_x was tested as an active RS oxide with promising results. Metal/SiO_x/Si structures have been shown to display resistive switching even for ultrathin SiO_x layers (~1 nm thick).[5] The associated physical mechanisms were related to the formation of conducting nanofilaments, either due to the reduction of Si atoms[6,7] or due to the drift/diffusion of the metallic electrode through the oxide layer.[8] These devices displayed excellent retention time, high ON/OFF ratio and multilevel storage potential.[9,10] Other reports account for a localized switching model involving proton exchange reactions, where resistive switching is related to an interplay between conductive Si-H-Si and non-conductive H-SiSi-H defects.[11–14] This effect was found to be stable at high temperatures.[11,14] On the other hand, it has been proposed that inserting an SiO_x layer in contact with other active memristive oxide such as ZnO changes the resistive switching behavior from bipolar to complementary (similar to the behavior of two serial RRAM devices with bipolar resistive switching in a back-to-back structure).[15] This effect seems to be strongly related to the oxygen storage capacity of the inserted SiO_x layer. A related scenario was proposed for TiN/SiO_2/Fe structures, where the presence of SiO_2 allows the spontaneous formation of FeO_x during the Fe deposition, which is ultimately responsible of the memristive behavior.[16] These works suggest that the RS behavior can be dramatically affected by combining two or more active oxides.

On the other hand, memristive behaviour in manganese oxides, usually known as "manganites," has been extensively studied in the last 15 years since the initial report of Ignatiev *et al.*[17] Phenomenological models that successfully describe

a)Author to whom correspondence should be addressed. Electronic mail: diego.rubi@gmail.com

the electrical behavior have been developed.[18,19] Proposed mechanisms associated with the memristive behavior in manganites include the modulation of the height of the Schottky (Sch) barrier at the oxide/metal interface,[20] the oxidation/reduction of a thin layer of the metallic electrode in contact with the manganite[21] and the creation/disruption of conducting (metallic) filaments bridging both electrodes.[20–22] Concerning electronic transport, different mechanisms such as Poole-Frenkel (PF),[23] space charged limited current (SCLC)[24] or Schottky (Sch) conduction[25,26] have been reported for manganite-based devices.

We have already faced the study of memristive TE/$La_{2/3}Ca_{1/3}MnO_3$ (TE: Ti/Cu with the thicknesses of 10 and 100 nm, respectively) devices grown on heavily doped n-Si (which acted as bottom electrode) without removing the native SiO_x layer.[20] A bipolar RS behavior was found with a crossover between two of the above mentioned mechanisms – modulation of the metal/manganite interface resistance and metallic filament formation – controlled by the compliance current (CC) programmed during the transition from high to low resistance states (SET process). We recall that in that work the applied electrical stress was *voltage* and only two stable resistance states (R_{HIGH} and R_{LOW}) were obtained. We argued that the time window of a few ms that the standard source-meters take to stabilize the CC leads to an uncontrolled power overshoot during the SET process (power $P = V^2/R$) that induces the hard dielectric breakdown of the SiO_x layer laying between the Si substrate and the manganite layer.[20,27] This unwanted effect could be avoided if the electrical stress is in the current controlled mode because the dissipated power during the SET process remains self limited ($P = I^2R$). This strategy has been followed in Ref. 28, where an intermediate resistance state (R_{INT}) was unveiled. This multilevel behavior could be related to a combination of the oxidation/reduction of the SiO_x ultrathin layer plus the formation of a (partial) metallic filament that does not bridge both the electrodes.[28,29] However, further evidence clarifying this physical mechanism is still needed.

In the present work, we report on impedance spectroscopy (IS) experiments performed on the different resistive states of the Ti/$La_{1/3}Ca_{2/3}MnO_3$/SiO_x/n-Si structures. Complemented with a careful analysis of the dynamical current-voltage curves, the IS analysis allows us conclusively setting the physical scenario associated with the multilevel resistive switching observed in these systems, in which the capability of the SiO_x layer for taking and releasing oxygen ions from and to the nearby manganite layer is proposed to play a key role. These results confirm that the combination of two active oxides improves the functionalities of the devices with respect to the single-oxide structures.

The $La_{1/3}Ca_{2/3}MnO_3$ manganite (LCMO) thin films were grown on top of heavily doped n-type silicon ($\delta < 5\,m\Omega\,cm$) by pulsed laser deposition. No chemical removal of the native SiO_x layer was performed. The thickness of this layer in an as-received substrate was estimated in ~1 nm by the X-ray photoemission spectroscopy (see supplementary material), although it may become thicker after heating the substrate in O_2 atmosphere in the chamber, prior to deposition. A 266 nm Nd:YAG solid state laser, operating at a repetition frequency of 10 Hz, was used. The deposition temperature and oxygen pressure were 850 °C and 0.13 mbar, respectively. The films resulted single phase and polycrystalline.[28] The film thickness was estimated by cross-section scanning electron microscopy imaging in 100 nm. Ti top electrodes (100 nm thick) were deposited by sputtering and shaped by means of optical lithography. Top electrode areas ranged between 32×10^3 μm^2 and 196×10^3 μm^2. Electrical characterization was performed at room temperature with a Keithley 2612 source-meter hooked to a probe station. The n-type silicon substrate was grounded and used as bottom electrode. The electrical stimulus was applied to the top electrode. Samples were electrically formed by applying a positive current of 2 mA, which starts the formation of a metallic filament and renders the device in a high resistance state.[28] Upon forming, the resistance changes from the virgin state $R_V \sim 2M\Omega$ to $R_{HIGH} \sim 60\,k\Omega$. Complex impedance was measured by using an AutoLab PGSTAT302N impedance analyzer at room temperature. A fixed AC signal of 100 mV was applied, with the frequencies between 10 Hz and 1 MHz.

Figures 1(a) and 1(b) display a dynamical current-voltage (I–V) curve and a hysteresis switching loop (HSL), respectively. The I–V curve is obtained by applying a sequence of current pulses of different amplitudes ($0 \rightarrow 17.5\,mA \rightarrow -16\,mA \rightarrow 0$, with a time-width of a few milliseconds and a step of 0.1 mA), while the voltage is measured during the application of the pulse. Additionally, after each current pulse, we apply a small undisturbing reading voltage of 100 mV that allows measuring the current and evaluating the remnant resistance state (HSL). The device is initially in R_{HIGH} and, upon positive stimulus, goes through two transitions, first to R_{LOW} (SET process) after a pulse of 2 mA and then to R_{INT} after a pulse of 14 mA. When the polarity of the stimulus is reversed, a transition from R_{INT} to R_{HIGH} (RESET process) is observed after a −16 mA pulse. Also, the transition from R_{LOW} to R_{HIGH} was obtained for negative bias. The three

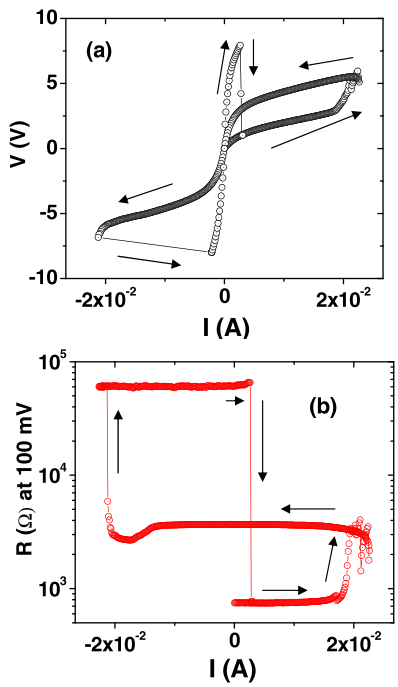

FIG. 1. (a) Current-voltage curve corresponding to a Ti/LCMO/SiO_2/n-Si device; (b) Hysteresis switching loops corresponding to the same device. Three non-volatile resistance levels are seen.

(remanent) resistance states (60 kΩ, 3.5 kΩ and 800 Ω) are clearly seen in the HSL of Figure 1(b). These resistance levels were stable for at least 10^4 s, and the device was found to display a reproducible behavior for at least 70 cycles.[28]

In order to gain information regarding the physical scenario behind the described phenomenology, we have performed complex impedance spectroscopy on the three resistance levels. This technique allows to characterize as a function of the frequency, the dielectric contribution from different regions of the device by modeling an equivalent electrical circuit. It has been already used to study the RS mechanisms in NiO, TiO_2, HfO_2 and amorphous Si based structures.[30,31] In particular, it was used as a tool to characterize the nature of conductive nanofilaments, as it permits to discriminate between "complete" filaments bridging both electrodes (ohmic resistors) and "incomplete" filaments, where exists a gap between the tip of the filament and the nearby electrode. In the latter case, the electrical behavior of the oxide in the gap is modeled by a capacitor in parallel with a resistor.[30,32] Recently, impedance spectroscopy was used in the memristive SiO_x-based systems to disclose the involved transport and switching mechanisms.[33]

Figure 2 displays the complex impedance spectra Z″ vs. Z′ (where Z″ and Z′ are the imaginary and real components of the complex impedance **Z**, respectively) associated with the R_{LOW}, R_{INT} and R_{HIGH} states. In the three cases, we observed semicircle-like curves, which can be accurately fitted by assuming an equivalent circuit constituted by a resistor (R_1) in series with two parallel resistor and capacitor combinations ($R_2//C_2$ and $R_3//C_3$), as shown in the sketch of Figure 3(a). We stress that no good fitting was obtained for other simpler equivalent circuits such as a single parallel resistor/capacitor combination (even in series with another resistor). The series resistor R_1 is related to the shift to the right of the diagram with respect to the origin of Z′ axis.

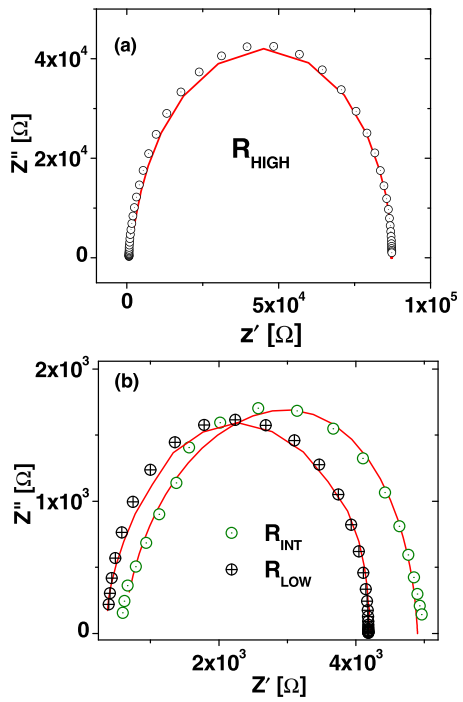

FIG. 2. (a), (b): Complex impedance spectra corresponding to the three resistance levels. Full red lines correspond to the fittings of the spectra.

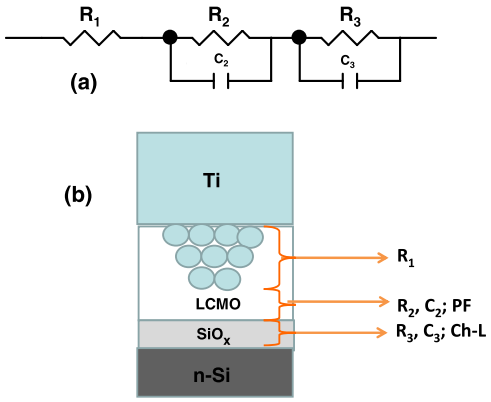

FIG. 3. (a) Equivalent circuit proposed for modeling the complex impedance spectra; (b) Sketch showing the physical scenario related to the equivalent circuit.

The fitted parameters for each resistance level are shown in Table I. As depicted in Figure 3(b), the obtained equivalent circuit is consistent with the existence of a metallic filament that does not connect both electrodes[30] and produced as a consequence of the migration of Ti^+ due to the positive polarity of the forming protocol. This Ti filament is represented by the series resistor R_1, while the parallel resistor/capacitor elements correspond to the manganite layer between the tip of the Ti filament and the native SiO_x, and to the SiO_x layer, respectively. The metallic filament is consistent with the lack of electrode area dependence of the R_{LOW} state,[28] while the existence of the gap between the tip of the filament and the bottom electrode is supported by the semiconductor-like temperature dependence of R_{LOW} (see Ref. 28 and supplementary material).

The observation of Table I shows that the three resistance states are nicely reflected in the fitted resistances values: the R_{HIGH} state is dominated by $R_3 \sim 85$ kΩ, which we attribute to the SiO_x layer after the positive polarity forming process. This value significantly drops to $R_3 \sim 1.5$ kΩ in the transition to R_{LOW}. Due to the positive polarity of the stimulus, the SiO_x layer becomes oxygen deficient giving rise to a lower value of R_3 (see below for more details). The transition from R_{LOW} to R_{INT} is dominated by the variation of R_2, which changes from ∼1.5 kΩ to ∼2 kΩ, indicating a change of the resistance of the manganite layer. There are concomitant changes of the capacitances C_1 from 4.5 to 3.5 nF and C_2 from 0.9 nF to 2nF. Changes in the capacitance after the application of electrical stress has been observed in the $LaAlO_3$-based memristive systems and were related to the modifications of the interfacial depletion layers due to oxygen movement.[34] Further studies are needed in our case to confirm this possible scenario. The slight variations in R_1 could be related to some minor filament reshaping produced during the resistive transitions.

TABLE I. Fitted circuit parameters for the three resistance levels.

	R_1 (Ω)	R_2 (Ω)	C_2 (nF)	R_3 (Ω)	C_3 (nF)
R_{HIGH}	800	1.5 k	4.5	85 k	0.7
R_{LOW}	400	1.5 k	4.5	2.3 k	0.9
R_{INT}	600	2 k	3.5	2.3 k	2

More information regarding the physics of the observed resistive transitions can be achieved by analyzing the dynamic I–V curves corresponding to the three resistive states, as shown in Figure 4(a) and recorded by applying stimuli (current again) in the "read" range, that is, not high enough to trigger the resistive transitions. An easy way to graphically analyze the I–V curves consists of plotting the power exponent γ as a function of $V^{1/2}$, where γ is defined as d(ln(I))/dln(V), as shown in Figures 4(b)–4(d). This is better than performing fits of the I–V curves with the usual non-linear mathematical expressions related to each particular conduction mechanism through the metal-oxide interfaces, as a constant value or a straight line dependence of γ with $V^{1/2}$ may reveal the conduction mechanism, without the need of numerically judging the quality of a fit.[35] This is particularly the case for both R_{HIGH} and R_{LOW}, where a constant value $\gamma \sim 3/2$ is observed, indicating a dominating Child-Langmuir (Ch-L) conduction mechanism.[36] A similar mechanism has been observed in the case of Al/SiO_2/n-Si devices.[37] In the Ch-L conducting regime, the current can be expressed as

$$I = \frac{AV^{3/2}}{d^2}, \tag{1}$$

where A is related to the permittivity of vacuum and with the electron's mass and charge, and d is the distance of the voltage drop. The switching from R_{HIGH} to R_{LOW} can then be ascribed to a decrease in d to $\sim d/10$, indicating the formation of a conducting channel that dramatically reduces the effective value of d but preserves the dominant conduction mechanism.

The graphic power exponent method is especially useful for the cases where two or more conduction mechanisms are present.[38] This is particularly what happens for the R_{INT} state, which shows a non-monotonic evolution of γ, displaying a characteristic shape that includes an almost constant initial value of 1 at low voltages, a linear increase and a cusp with $\gamma \sim 4$ for $V^{1/2} \sim 2.2$ $V^{1/2}$. As shown in Ref. 38, this shape of the γ curve indicates the existence of a PF emission, which dominates the conduction mechanism in the intermediate current-voltage regime, in parallel with an ohmic element, and both in series with a lower γ process, visible at higher voltages, possibly related to the Ch-L conduction observed for R_{HIGH} and R_{LOW}.

We recall that the PF conduction mechanism is a bulk process related to the electronic emission of carriers from traps in the oxide.[36] It can be found typically in the interfaces of metal-complex oxides, such as cuprates or cobaltites.[39,40] In this way, its origin can be related to the LCMO layer, which contributes with a pure ohmic conduction in the R_{HIGH} and R_{LOW} regimes, but becomes Poole-Frenkel after the $R_{LOW} \rightarrow R_{INT}$ transition, due to the generation of defects (traps).

Within this framework, we propose the following physical scenario, as shown in Figure 3(b): after the initial positive electroforming, an incomplete metallic filament is formed and the device is stabilized in the R_{HIGH} resistance level, where the device resistance is dominated by the SiO_x layer (with x close to the stoichiometric value 2) and the Ch-L conduction mechanism originating in this layer prevails. The application of positive stimulus leads into the SET transition (R_{HIGH} to R_{LOW}), which is related to oxygen transfer from the SiO_x to the manganite layers. In the case of SiO_x, it is known that the electrical conductance is enhanced if the oxygen stoichiometry is reduced. This is reflected by the abrupt decrease in R_3. The conduction mechanism in the R_{LOW} state is still dominated by the SiO_x layer, remaining Ch-L type but with an enhanced conducting channel, consequence of its lower oxygen stoichiometry. Upon the application of further positive stimulus, more oxygen ions are transferred from the SiO_x to the manganite layer, stabilizing the R_{INT} state. In

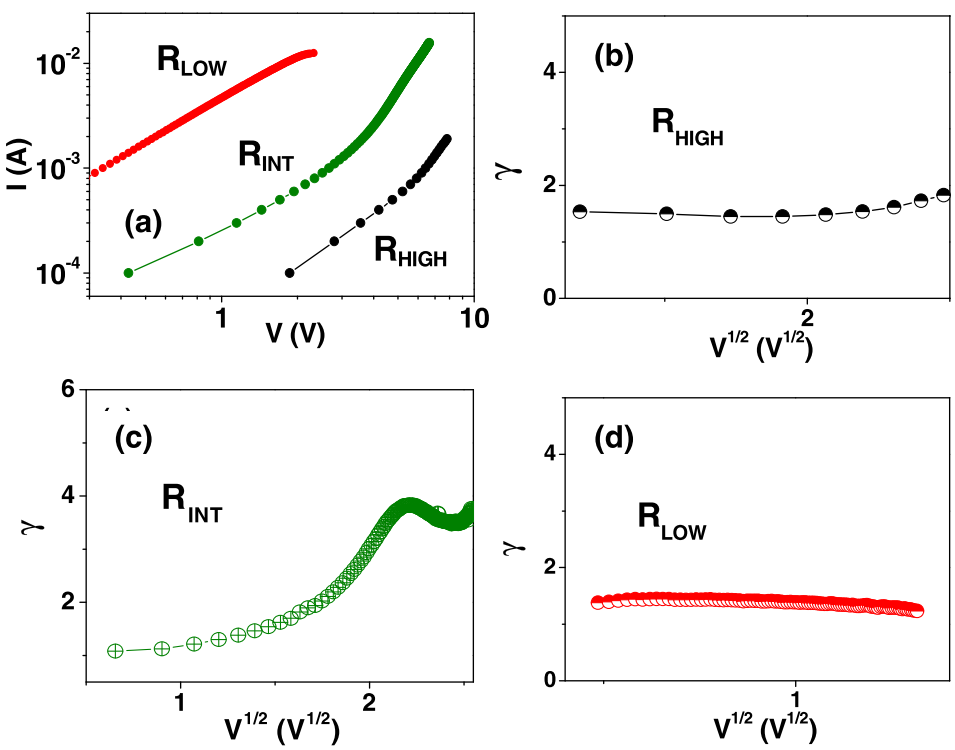

FIG. 4. (a) Current-voltage curves corresponding to the three resistance levels for low stimulus ("reading" range); (b), (c), (d) Evolution of $\gamma = d(\ln(I))/d\ln(V))$ as a function of $V^{1/2}$, for the three resistance levels.

this state, the conduction mechanism starts being dominated by the manganite layer. It can be argued that the transfer of oxygen ions from the SiO_x to the manganite layer fill oxygen vacancies and above a certain threshold ($R_{LOW} \rightarrow R_{INT}$, reflected by an increase in R_2) forms trap-centers, increasing the manganite resistance and stabilizing the Poole-Frenkel conduction mechanism that dominates the macroscopic transport. The application of negative stimulus reverses the processes already described; oxygen is transferred back from the manganite to the SiO_x layer that becomes more stoichiometric and returns to R_{HIGH}, and the dominating conduction mechanism becomes Ch-L again.

In summary, we have conclusively disclosed the physical scenario associated with the three-level resistive switching in n-Si/SiO_x/LCMO/Ti devices. The contribution of three regions (metallic filament, manganite and SiO_x layers) to the transport properties has been individualized. Our results show that the existence of the native SiO_x layer plays a key role in the stabilization of an intermediate resistance level, indicating that the combination of two or more active RS oxides in single devices improves their functionalities. We understand that these multilevel devices are interesting and promising as their fabrication procedure is rather simple and they are fully compatible with the standard Si-based electronics.

See supplementary material for the X-ray photoemission spectroscopy characterization of an as received Si substrate and the temperature dependence of R_{LOW}, R_{HIGH} and R_{INT}.

We acknowledge the financial support from CONICET (PIP 291), PICT "MeMO"(0788) and CIC-Buenos Aires. We thank U. Lüders and J. Lecourt, from CRISMAT, for the preparation of the manganite target and P. Granell, from INTI, for the SEM-FIB measurements. We also thank S. Bengió, from CAB-Bariloche, for the XPS measurement. We thank H. Corti and his group for the access to the impedance analyzer.

[1]A. Sawa, Mater. Today **11**, 28 (2008).
[2]R. Waser, R. Dittmann, G. Staikov, and K. Szot, Adv. Mater. **21**, 2632 (2009).
[3]S. H. Jo, T. Chang, I. Ebong, B. B. Bhadviya, P. Mazumder, and W. Lu, Nano Lett. **10**, 1297 (2010).
[4]Y. F. Chang, B. Fowler, Y. C. Chen, F. Zhou, C. H. Pan, T. C. Chang, and J. C. Lee, Sci. Rep. **6**, 21268 (2016).
[5]C. Li, H. Jiang, and Q. Xia, Appl. Phys. Lett. **103**, 062104 (2013).
[6]J. Yao, J. Lin, Y. Dai, G. Ruan, Z. Yan, L. Li, L. Zhong, D. Natelson, and J. M. Tour, Nat. Commun. **3**, 1101 (2012).
[7]J. Yao, Z. Sun, L. Zhong, D. Natelson, and J. M. Tour, Nano Lett. **10**, 4105 (2010).
[8]H. Sun, Q. Liu, S. Long, H. Lv, W. Banarjee, and M. Liu, J. Appl. Phys. **116**, 154509 (2014).
[9]F. Zhou, Y. F. Chang, B. Fowler, K. Byun, and J. C. lee, Appl. Phys. Lett. **106**, 063508 (2015).
[10]A. Mehonic, S. Cueff, M. Wodjak, S. Hudziak, C. labbe, R. Rizk, and A. J. Keyon, Nanotechnology **23**, 455201 (2012).
[11]Y. F. Chang, B. Fowler, Y. C. Chen, Y. T. Chen, Y. Wang, F. Xue, F. Zhou, and J. C. Lee, J. Appl. Phys. **116**, 043708 (2014).
[12]Y. F. Chang, B. Fowler, Y. C. Chen, Y. T. Chen, Y. Wang, F. Xue, F. Zhou, and J. C. Lee, J. Appl. Phys. **116**, 043709 (2014).
[13]B. Fowler, Y. F. Chang, F. Zhou, Y. Wang, P. Y. Chen, F. Xue, Y. T. Chen, B. Bringhurst, S. Pozder, and J. C. Lee, RSC Adv. **5**, 21215 (2015).
[14]F. Zhou, Y. F. Chang, Y. C. Chen, X. Wu, Y. Zhang, B. Fowler, and J. C. Lee, Phys. Chem. Chem. Phys. **18**, 700 (2016).
[15]Y. T. Tseng, T. M. Tsai, T. T. Chang, C. C. Shih, K. C. Chang, R. Zhang, K. H. Chen, J. H. Chen, Y. C. Li, C. Y. Lin, Y. C. Hung, Y. E. Syu, J. C. Zheng, and S. M. Sze, Appl. Phys. Lett. **106**, 213505 (2015).
[16]L. W. Feng, C. Y. Chang, Y. F. Chang, W. R. Chen, S. Y. Wang, P. W. Chiang, and T. C. Chang, Appl. Phys. Lett. **96**, 052111 (2010).
[17]S. Q. Liu, N. J. Wu, and A. Ignatiev, Appl. Phys. Lett. **76**, 2749 (2000).
[18]M. Rozenberg, M. J. Sánchez, R. Weht, C. Acha, F. G. Marlasca, and P. Levy, Phys. Rev. B **81**, 115101 (2010).
[19]W. Román Acevedo, D. Rubi, F. G. Marlasca, F. Golmar, U. Lüders, J. Lecourt, J. Suñé, P. Levy, and E. Miranda, in 2015 International Conference on Memristive Systems (MEMRISYS) (IEEE, 2016).
[20]D. Rubi, F. Tesler, I. Alposta, A. Kalstein, N. Ghenzi, F. Gomez-Marlasca, M. Rozenberg, and P. Levy, Appl. Phys. Lett. **103**, 163506 (2013).
[21]A. Herpers, C. Lenser, C. Park, F. Offi, F. Borgatti, G. Panaccione, S. Menzel, R. Waser, and R. Dittmann, Adv. Mater. **26**, 2730 (2014).
[22]D. Rubi, A. Kalstein, W. S. Román, N. Ghenzi, C. Quinteros, E. Mangano, P. Granell, F. Golmar, F. G. Marlasca, S. Suárez, G. Bernardi, C. Albornoz, A. G. Leyva, and P. Levy, Thin Solid Films **583**, 76 (2015)
[23]D. Shang, L. Chen, Q. Wang, W. Zhang, Z. Wu, and X. M. Li, Appl. Phys. Lett. **89**, 172102 (2006).
[24]W. Yu, X. Li, F. Wu, D. Shang, and L. Chen, Proc. SPIE **6984**, 698439 (2008).
[25]Z. Yan and J. Liu, Ann. Phys. **358**, 206 (2015).
[26]M. Wu, C. Yang, D. Shi, R. Wang, L. Xu, H. Xiao, and K. Baerner, AIP Adv. **4**, 047123 (2014).
[27]K. Komiya and Y. Omura, J. Semicond. Technol. Sci. **2**, 164 (2002).
[28]W. Román Acevedo, D. Rubi, J. Lecourt, U. Lüders, F. Gómez-Marlasca, P. Granell, F. Golmar, and P. Levy, Phys. Lett. A **380**, 2870 (2016).
[29]N. Ghenzi, M. J. Sánchez, D. Rubi, M. J. Rozenberg, C. Urdaniz, M. Weissman, and P. Levy, Appl. Phys. Lett. **104**, 183505 (2014).
[30]X. L. Jiang, Y. G. Zhao, Y. S. Chen, D. Li, Y. X. Luo, D. Y. Zhao, Z. Sun, J. R. Sun, and H. W. Zhao, Appl. Phys. Lett. **102**, 253507 (2013).
[31]Y. Liu, P. Gao, X. Jiang, K. Bi, H. Xu, and W. Peng, Appl. Phys. Lett. **104**, 043502 (2014).
[32]Y. H. You, B. S. So, and J. H. Hwang, Appl. Phys. Lett. **89**, 222105 (2006).
[33]Y. F. Chang, B. Fowler, Y. C. Chen, and J. C. Lee, Prog. Solid State Chem. **44**, 75 (2016).
[34]S. X. Wu, H. Y. Peng, and T. Wu, Appl. Phys. Lett. **98**, 093503 (2011).
[35]A. Bozhko, M. Shupegin, and T. Takagi, Diamond Relat. Mater. **11**, 1753 (2002).
[36]S. M. Sze and K. K. Ng, *Physics of Semiconductor Devices* (John Wiley & Sons, 2006).
[37]S. Srisonphan, Y. S. Jung, and H. K. Kim, Nat. Nanotechnol. **7**, 504–508 (2012).
[38]C. Acha, e-print arXiv.org/abs/1609.04472.
[39]A. Schulman, L. F. Lanosa, and C. Acha, J. Appl. Phys. **118**, 044511 (2015).
[40]C. Acha, A. Schulman, M. Boudard, K. Daoudi, and T. Tsuchiya, Appl. Phys. Lett. **109**, 011603 (2016).